Cell

Iron-Export Ferroxidase Activity of β-Amyloid Precursor Protein Is Inhibited by Zinc in Alzheimer's Disease

James A. Duce,[1] Andrew Tsatsanis,[1] Michael A. Cater,[1,9] Simon A. James,[1] Elysia Robb,[1] Krutika Wikhe,[1] Su Ling Leong,[3,4] Keyla Perez,[1,3,4] Timothy Johanssen,[4] Mark A. Greenough,[1,2] Hyun-Hee Cho,[5] Denise Galatis,[3] Robert D. Moir,[6] Colin L. Masters,[1] Catriona McLean,[7] Rudolph E. Tanzi,[6] Roberto Cappai,[3,4] Kevin J. Barnham,[1,3,4] Giuseppe D. Ciccotosto,[1,3,4] Jack T. Rogers,[4,5,8,*] and Ashley I. Bush[1,3,8,*]

[1]Mental Health Research Institute, The University of Melbourne, Parkville, Victoria 3052, Australia
[2]Department of Genetics
[3]Department of Pathology
[4]Bio21 Molecular Science and Biotechnology Institute
The University of Melbourne, Victoria 3010, Australia
[5]Neurochemistry Laboratory, Department of Psychiatry, Harvard Medical School
[6]Genetics and Aging Research Unit
Massachusetts General Hospital, Charlestown, MA 02129, USA
[7]Department of Anatomical Pathology, Alfred Hospital, Melbourne, Victoria 3004, Australia
[8]These authors contributed equally to this work
[9]Present address: Research Division, The Peter MacCallum Cancer Centre, St. Andrew's Place, East Melbourne, Victoria 3002, Australia
*Correspondence: jrogers@partners.org (J.T.R.), abush@mhri.edu.au (A.I.B.)
DOI 10.1016/j.cell.2010.08.014

SUMMARY

Alzheimer's Disease (AD) is complicated by pro-oxidant intraneuronal Fe^{2+} elevation as well as extracellular Zn^{2+} accumulation within amyloid plaque. We found that the AD β-amyloid protein precursor (APP) possesses ferroxidase activity mediated by a conserved H-ferritin-like active site, which is inhibited specifically by Zn^{2+}. Like ceruloplasmin, APP catalytically oxidizes Fe^{2+}, loads Fe^{3+} into transferrin, and has a major interaction with ferroportin in HEK293T cells (that lack ceruloplasmin) and in human cortical tissue. Ablation of APP in HEK293T cells and primary neurons induces marked iron retention, whereas increasing APP695 promotes iron export. Unlike normal mice, $APP^{-/-}$ mice are vulnerable to dietary iron exposure, which causes Fe^{2+} accumulation and oxidative stress in cortical neurons. Paralleling iron accumulation, APP ferroxidase activity in AD postmortem neocortex is inhibited by endogenous Zn^{2+}, which we demonstrate can originate from Zn^{2+}-laden amyloid aggregates and correlates with Aβ burden. Abnormal exchange of cortical zinc may link amyloid pathology with neuronal iron accumulation in AD.

INTRODUCTION

In Alzheimer's disease (AD), Zn^{2+} collects with β-amyloid (Aβ) in hallmark extracellular plaques (Adlard et al., 2008; Cherny et al., 1999; Lee et al., 2002; Lovell et al., 1998; Miller et al., 2006; Suh et al., 2000), adjacent to neocortical neurons filled with pro-oxidant Fe^{2+} (Bartzokis et al., 1994a, 1994b; Bartzokis and Tishler, 2000; Honda et al., 2005). The elevated neuronal iron exacerbates the pervasive oxidative damage that characterizes AD and may foster multiple pathologies including tau-hyperphosphorylation and neurofibrillary tangle formation (Honda et al., 2005; Smith et al., 1997; Yamamoto et al., 2002), but the cause of this neuronal iron elevation is unknown.

Aβ is derived from a broadly expressed type I transmembrane protein precursor (APP) of uncertain function and constitutively cleaved into various fragments. The 5′ untranslated region (UTR) of APP mRNA possesses a functional iron-responsive element (IRE) stem loop with sequence homology to the IREs for ferritin and transferrin receptor (TFR) mRNA (Rogers et al., 2002). APP translation is thus responsive to cytoplasmic free iron levels (the labile iron pool, LIP), which also govern the binding of iron regulatory proteins (IRPs) to ferritin and TFR mRNA in a canonical *cis-trans* iron regulatory system (Klausner et al., 1993). When cellular iron levels are high, translation of APP and the iron-storage protein ferritin is increased (Rogers et al., 2002), whereas RNA for the iron importer TFR is degraded.

Ferroxidases prevent oxidative stress caused by Fenton and Haber-Weiss chemistry by oxidizing Fe^{2+} to Fe^{3+}. Losses of ferroxidase activities cause pathological Fe^{2+} accumulation and neurodegenerative diseases, such as aceruloplasminemia where mutation of the multicopper ferroxidase ceruloplasmin (CP) leads to glial iron accumulation and dementia (Chinnery et al., 2007; Harris et al., 1995; Mantovan et al., 2006; Patel et al., 2002). Iron-export ferroxidases CP and hephaestin interact with ferroportin and facilitate the removal (e.g., by transferrin) of cytoplasmic iron translocated to the surface by ferroportin

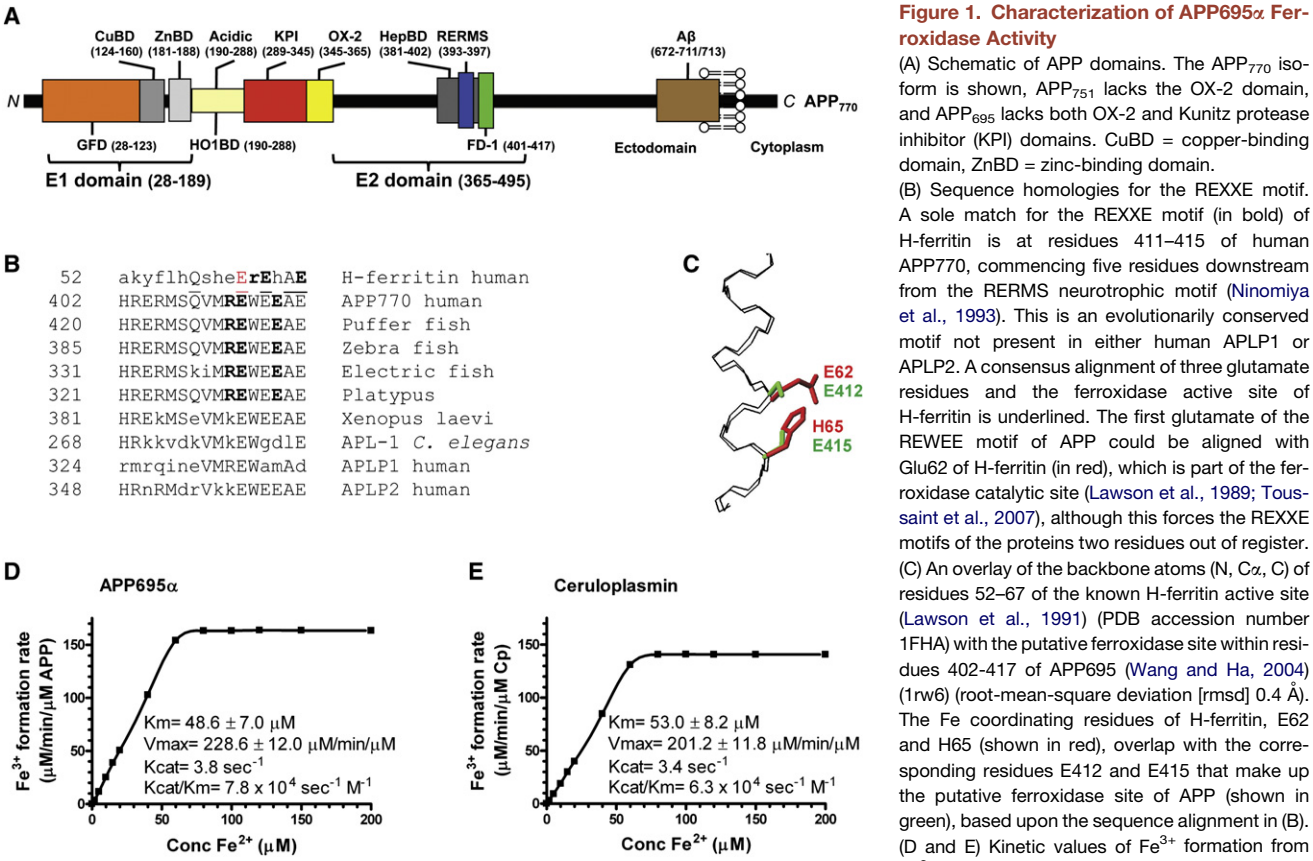

Figure 1. Characterization of APP695α Ferroxidase Activity

(A) Schematic of APP domains. The APP_{770} isoform is shown, APP_{751} lacks the OX-2 domain, and APP_{695} lacks both OX-2 and Kunitz protease inhibitor (KPI) domains. CuBD = copper-binding domain, ZnBD = zinc-binding domain.

(B) Sequence homologies for the REXXE motif. A sole match for the REXXE motif (in bold) of H-ferritin is at residues 411–415 of human APP770, commencing five residues downstream from the RERMS neurotrophic motif (Ninomiya et al., 1993). This is an evolutionarily conserved motif not present in either human APLP1 or APLP2. A consensus alignment of three glutamate residues and the ferroxidase active site of H-ferritin is underlined. The first glutamate of the REWEE motif of APP could be aligned with Glu62 of H-ferritin (in red), which is part of the ferroxidase catalytic site (Lawson et al., 1989; Toussaint et al., 2007), although this forces the REXXE motifs of the proteins two residues out of register.

(C) An overlay of the backbone atoms (N, Cα, C) of residues 52–67 of the known H-ferritin active site (Lawson et al., 1991) (PDB accession number 1FHA) with the putative ferroxidase site within residues 402-417 of APP695 (Wang and Ha, 2004) (1rw6) (root-mean-square deviation [rmsd] 0.4 Å). The Fe coordinating residues of H-ferritin, E62 and H65 (shown in red), overlap with the corresponding residues E412 and E415 that make up the putative ferroxidase site of APP (shown in green), based upon the sequence alignment in (B).

(D and E) Kinetic values of Fe^{3+} formation from Fe^{2+} monitored by incorporation into transferrin, indicated within the graphs, were calculated for each protein (200 nM) incubated with various concentrations of Fe^{2+} at pH 7.2 to reflect the normal pH of brain interstitial space, where apo-transferrin is abundant (Visser et al., 2004). CP values are in close agreement with the original reports (Osaki, 1966).

Data are means ± standard error of the mean (SEM), n = 3 replicates, typical of three experiments. See also Figure S1.

(De Domenico et al., 2007). Their expression is cell specific (e.g., CP in glia, hephaestin in gut epithelia), but an iron-export ferroxidase for neocortical neurons is unknown (Klomp et al., 1996). CP is expressed in GPI-anchored and soluble forms (De Domenico et al., 2007; Jeong and David, 2003; Patel et al., 2002). APP similarly is expressed in transmembrane and secreted forms. We explored whether APP is a ferroxidase and in turn has a role in neuronal iron export—an activity consistent with APP translation being responsive to iron levels. We also tested whether, in AD, APP ferroxidase activity is altered in a manner linked to the accumulation of its Aβ derivative in plaque pathology.

RESULTS

APP695 Possesses Ferroxidase Activity Similar to Ceruloplasmin

We noted that APP possesses a REXXE ferroxidase consensus motif (Gutierrez et al., 1997) as found in the ferroxidase active site of H-ferritin (Figures 1A and 1B). This evolutionarily conserved motif is not present in paralogs APLP1 or 2 (Figure 1B). There is good structural homology between the known 3D structures of H-ferritin (Lawson et al., 1991) and the REXXE region of the E2 domain of APP (Wang and Ha, 2004), with low root-mean-square deviation (0.4 Å) when overlaying backbone atoms of the α-helical H-ferritin catalytic site (residues 52–67) with the corresponding backbone atoms of APP (residues 402–417) (Figure 1C). The homology extends to the side chains constituting the Fe coordinating residues of H-ferritin, E62, and H65, which overlap with potential Fe coordinating residues E412 and E415 of APP695 (Figure 1C).

Recombinant soluble APP695α, representing the predominant neuronal APP species (Rohan de Silva et al., 1997), possessed robust ferroxidase activity (V_{max} = 228.6 μM Fe^{3+}/min/μM APP; K_m = 48.6 μM; Figure 1D), like CP (Figure 1E), as measured by the rate of Fe^{3+} incorporation into transferrin. Therefore, APP is a more active ferroxidase than ferritin (V_{max} = 2.21 μM Fe^{3+}/min/μM ferritin, K_m = 200 μM) (Bakker and Boyer, 1986). APP695α ferroxidase activity was maintained across a pH range 5.0–9.0 (Figure S1A available online). APLP2 was inactive (Figure 2A), like the negative control albumin (Figure S1B), consistent with the absence of the REXXE motif (Figure 1B).

CP ferroxidase activity is dependent on copper and inhibited by NaN_3 (Osaki, 1966). Neither NaN_3 (Figure 2A) nor Cu^{2+} (2:1 Cu:APP, not shown) altered APP695α activity, indicating that APP695α ferroxidase chemistry is like H-ferritin (Bakker and

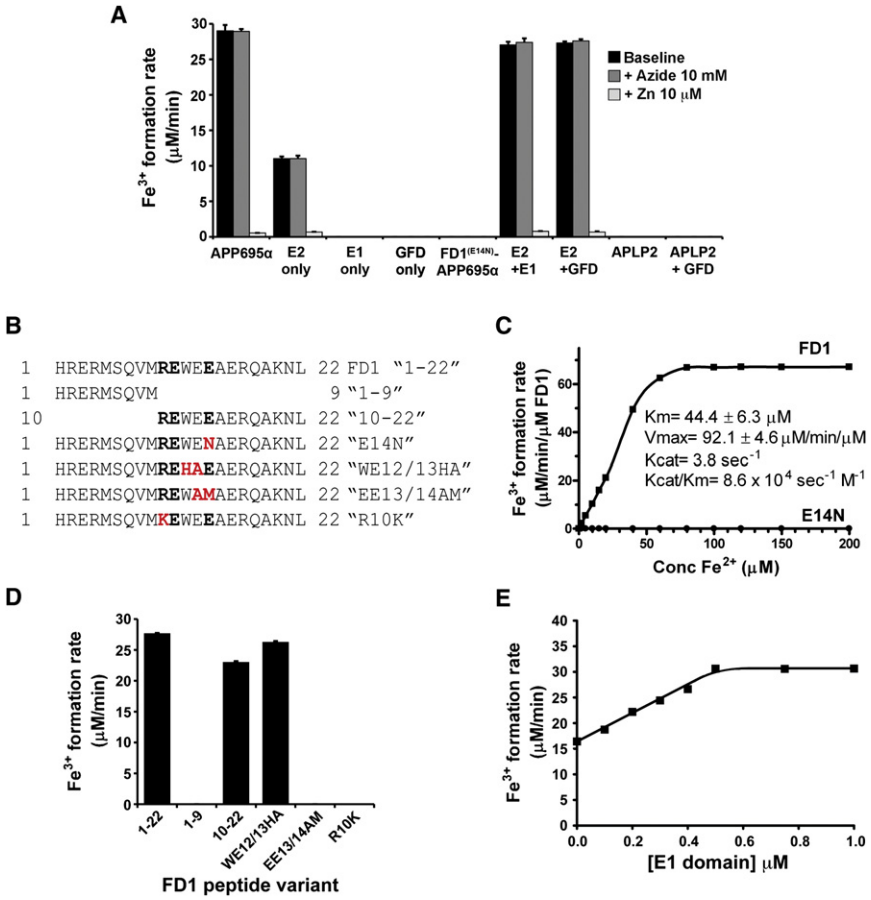

Figure 2. Domains Important to APP Ferroxidase Activity and Its inhibition by Zn^{2+}

(A) Activities of the E2 fragment of APP ± GFD-containing fragments compared to APP695α, FD1$^{(E14N)}$-APPα, and APLP2α in HBS (pH 7.2). Effects of ferroxidase inhibitors NaN_3 (10 mM) for CP and Zn^{2+} (10 μM) for H-ferritin are shown. FD1$^{(E14N)}$-APP695α has the mutation in the REXXE motif shown in Figures 2B and 2C.

(B) Sequences of FD1 and derived peptides used to map the active site of APP695α. The REXXE motif is in bold, and the substitution site in red. The last three peptides have substitutions in the putative active site that represent the homologous sequences of H-ferritin, APLP1, and APLP2, respectively.

(C) Ferroxidase activities of a 22 residue peptide containing the REXXE consensus motif of APP ("FD1," see B) and the same peptide where the REWEE sequence is substituted with REWEN ("E14N," see B).

(D) Ferroxidase activity of FD1 is specific to the REXXE motif. Activity is retained upon deleting the first nine residues (containing the RERMS motif), and when the H-ferritin REXXE consensus motif is substituted into the peptide (WE12/13HA). Activity is eliminated by substitution of the APLP1 (EE13/14AM) and APLP2 (R10K) sequences, which disrupt the REXXE consensus sequence. All peptides were 0.5 μM.

(E) Ferroxidase activity of the E2 domain of APP (0.5 μM) is potentiated by the E1 domain in a concentration-dependent manner up to a 1:1 stoichiometry.

Values are means ± SEM, n = 3 replicates, typical of three experiments. See also Figure S1.

Boyer, 1986) and not like CP. H-ferritin ferroxidase activity is inhibited by Zn^{2+} (Bakker and Boyer, 1986), and indeed Zn^{2+} inhibited the activities of both APP695α and the E2 domain of APP (Figure 2A). Inhibition was specific for Zn^{2+} among physiological divalent metal ions, given that Ca^{2+} (2 mM), Mg^{2+} (0.5 mM), Cu^{2+} (20 μM), Mn^{2+} (10 μM), Ni^{2+} (20 μM), and Co^{2+} (20 μM), as chloride salts, did not inhibit APP695α ferroxidase activity (not shown). The activities of the main isoforms, APP695α, APP770α, and APP751α, were identical (Figure S1C).

A 22 residue synthetic peptide within the E2 domain (FD1) (Figure 1A and Figure 2B), containing the putative active site of APP, possessed ferroxidase activity that was ~40% that of APP695α (Figure 2C). Mutational analysis of APP695α (Figure 2A) and FD1 (Figures 2B–2D) confirmed that disruption of the REXXE motif, by altering a single conserved amino acid (REWEN, "E14N" in Figures 2B and 2C), or substituting the homologous pentapeptide regions of APLP1 (REWAM, "EE13/14AM" in Figure 2D) or APLP2 (KEWEE, "R10K" in Figure 2D), abolished activity. Substitution with the homologous H-ferritin sequence (REHAE, "WE12/13HA" in Figure 2B), which does not disrupt the consensus motif, retained activity (Figure 2D).

Like FD1 peptide (Figure 2C), purified E2 polypeptide (Figure 1A) possessed ~40% of the ferroxidase activity of APP695α (Figure 2A). We explored for other domains of APP needed to restore full activity to E2. Whereas purified E1 domain possessed no ferroxidase activity, equimolar concentrations of E1 doubled E2 activity (Figure 2E) to about that of APP695α (Figure 2A). We mapped this potentiation effect to the growth factor domain (GFD) within E1 (Rossjohn et al., 1999) (Figure 2A). GFD did not engender activity from APLP2 (Figure 2A), consistent with the requirement for the REXXE motif.

APP Facilitates Iron Export and Interacts with Ferroportin

We hypothesized that APP ferroxidase activity may facilitate iron movement analogous to the interaction of CP with ferroportin (De Domenico et al., 2007). Ferroportin may be expressed in all cells, but CP is not, leading us to suspect that APP may play the ferroxidase role in certain cells that lack CP such as HEK293T (De Domenico et al., 2007) and cortical neurons (Klomp et al., 1996). The impact of endogenous APP suppression by RNAi on iron export was therefore initially studied in HEK293T cells, where the absence of CP was confirmed by western blot (not shown). APP-suppressed cells accumulated significantly more (~50%, $p < 0.01$) radioactive iron (^{59}Fe) than sham RNAi controls (Figure 3A and Figure S2A). Addition of APP695α (2 μM, Figure 3B) or the E2 domain of APP (2 μM, Figure S2A) to the media, after incorporation of ^{59}Fe into the cells, significantly promoted the efflux of ^{59}Fe into the media. E2 lacks the heme-oxygenase (HO) inhibitory domain of APP (Takahashi et al., 2000) (Figure 1A), and therefore APP is not promoting iron export in these cells merely through inhibition of

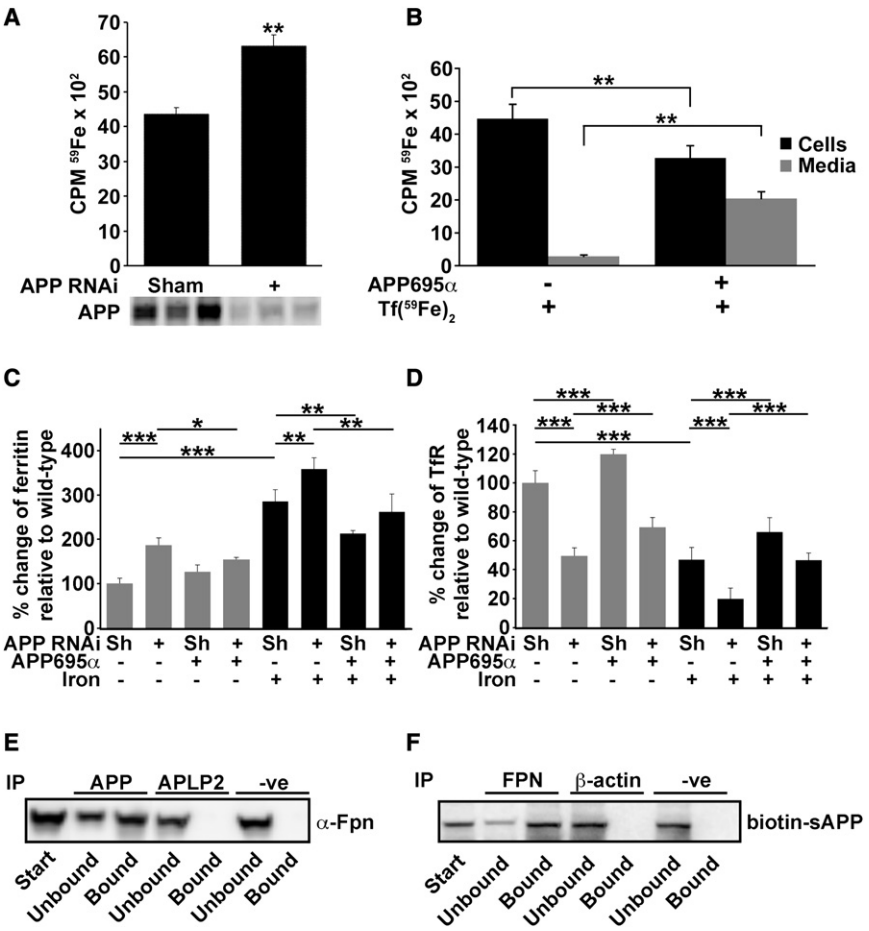

Figure 3. APP Promotes Iron Release, Lowers the Labile Iron Pool, and Interacts with Ferroportin in HEK293T Cells

(A) Iron flux was measured after incorporation of Tf ($^{59}Fe)_2$. APP RNAi (versus nonspecific scrambled RNAi, "sham") induces cellular ^{59}Fe retention. Suppression of APP, in triplicate, was confirmed by western blot (22C11).

(B) APP695α (2 μM) added to the media promotes ^{59}Fe export over 6 hr.

(C and D) Western blot (as shown in Figure S2B) quantification: APP RNAi increased ferritin (to ~200%) and decreased TFR levels (to ~50%), whereas APP695α partially reversed these effects. Additional iron ($Fe(NH_4)_2(SO_4)_2$,10 μM) raised the baseline ferritin and lowered the TFR, but the effect of adding or subtracting APP was similar. Sh = "sham," nonspecific scrambled RNAi.

(E) Interaction of APP with ferroportin using anti-FPN for detection and anti-N-terminal APP for immunoprecipitation of HEK293T cells treated with iron (10 μM). No interaction with APLP2 confirmed specificity to APP. Nonspecific rabbit IgG was used as a control ("-ve").

(F) Biotin-labeled APP695α, when added to the media of HEK293T cells treated with Fe $(NH_4)_2(SO_4)_2$ (10 μM), is immunoprecipitated from the cell homogenate with anti-FPN antibody.

Data are means ± SEM of n = 3. * = $p < 0.05$, ** = $p < 0.01$, *** = $p < 0.001$; (A) and (B) analyzed by two-tailed t tests, (C) and (D) by ANOVA + Dunnet's tests. See also Figure S2.

HO. Complementary changes in cellular levels of the iron-responsive proteins ferritin and TFR (Figures 3C and 3D, blots in Figure S2B), consistent with decreased IRP1 and 2 binding to a biotinylated IRE probe (Figure S2C), confirmed that APP acted to lower the LIP. As a further control, we studied the impact of stable transfection of wild-type (WT) or inactive mutant ($FD1^{(E14N)}$-APP695, Figure 2A) APP695 on iron retention in HEK293T cells. APP695 significantly decreased iron retention compared to cells transfected with vector alone, but $FD1^{(E14N)}$-APP695 increased iron retention, consistent with competition against endogenous APP (Figures S2D–S2F). These data indicate that ferroxidase-active APP facilitates iron export in HEK293T cells.

CP coimmunoprecipitates with ferroportin in certain tissues (De Domenico et al., 2007; Jeong and David, 2003). Analogously, most of the ferroportin in HEK293T cells coimmunoprecipitated with endogenous APP (Figure 3E, Figure S2G). Furthermore, the majority of a biotinylated APP695α probe added to HEK293T cells coimmunoprecipitated with ferroportin (Figure 3F), consistent with exogenous APP695α promoting iron export (Figures 3B–3D) by interacting with ferroportin.

We next studied iron transport in primary cortical neurons from $APP^{-/-}$ mice. $APP^{-/-}$ neurons retained significantly more ^{59}Fe than WT neurons (+50%, $p < 0.01$) (Figure 4A) and exhibited a corresponding decrease (−60%) in the rate of iron efflux (Figure 4B). The increased retention of iron in $APP^{-/-}$ neurons was comparable to that reported for $CP^{-/-}$ astrocytes over the same 12 hr incubation period (De Domenico et al., 2007; Jeong and David, 2003). APP695α added to WT neurons induced a significant concentration-dependent decrease in ^{59}Fe retention (Figure S3A) and reversed much of the increased ^{59}Fe retention in $APP^{-/-}$ neurons (Figure 4A). Inactive $FD1^{(E14N)}$-APP695α (Figure 2A) could not promote iron efflux (Figure S3B).

The E2 domain of APP also facilitated iron efflux in primary neuronal cultures (Figure S3C). As with APP-suppressed HEK293T cells (Figures 3C and 3D), more ferritin and less TFR were detected in $APP^{-/-}$ compared to WT neurons, exaggerated by the addition of 10 μM iron (Figure 4C, westerns shown in Figure S3D), consistent with increased neuronal iron. We confirmed (Figure S3D) that neocortical neurons do not express CP (Klomp et al., 1996). Therefore, cortical neurons may depend upon APP as the ferroxidase partner for ferroportin. Consistent with this, APP in human and mouse cortical tissue (including full-length membrane-bound APP) had a major interaction with ferroportin in immunoprecipitation studies (Figures 4D and 4E; Figures S4A–S4C). APLP2 did not coimmunoprecipitate with ferroportin from these tissues (Figure 4D).

Neocortical ferroportin also coimmunoprecipitated with CP (Figure 4D). This was expected because despite being absent

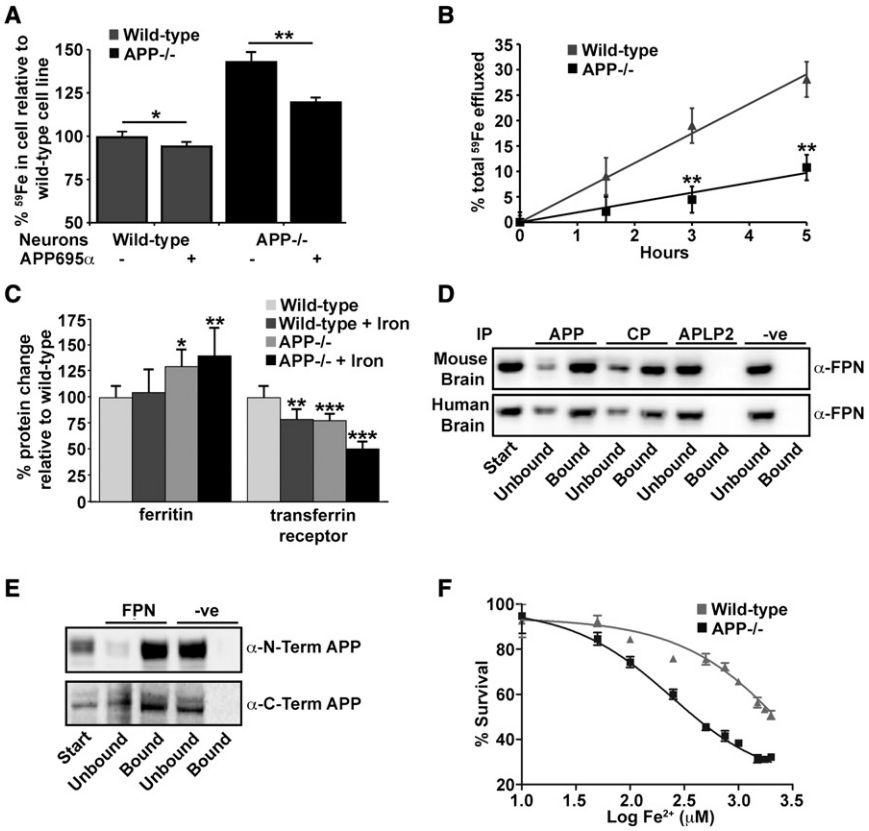

Figure 4. Intracellular Iron Accumulates in APP$^{-/-}$ Neurons

(A) APP$^{-/-}$ primary neurons treated with Tf(^{59}Fe)$_2$ retain more ^{59}Fe after 12 hr than cells from WT controls. APP695α (2 μM) promotes ^{59}Fe export into the media after 12 hr from both WT and APP$^{-/-}$ neurons. In APP$^{-/-}$ neurons this reduces intracellular iron to approach WT levels.

(B) ^{59}Fe media efflux is decreased for APP$^{-/-}$ compared to WT primary neurons. Data are ^{59}Fe counts in media expressed as a fraction of the total in culture.

(C) Western blot (see Figure S3D) quantification of ferritin and TFR in primary neuronal cultures from WT and APP$^{-/-}$ matched controls treated ± Fe$(NH_4)_2(SO_4)_2$ (75 μM). Differences in APP$^{-/-}$ cells are consistent with increased retention of iron.

(D) APP and CP coimmunoprecipitate with ferroportin from human and mouse brain, but not APLP2.

(E) Determination that membrane-bound full-length APP interacts with ferroportin using APP detection antibodies for both the N- and C-terminal ends of the protein from membrane lysate of human brain immunoprecipitated by anti-FPN antibody.

(F) APP$^{-/-}$ neurons incubated with increasing concentrations of $Fe(NH_4)_2(SO_4)_2$ are more susceptible to iron toxicity, measured by CCK-8 cell viability assay, than WT neurons.

Data are means ± SEM, n = 3, * = $p < 0.05$, ** = $p < 0.01$, *** = $p < 0.001$. (A)–(C) analyzed by two-tailed t tests, (D) by ANOVA + Dunnet's test compared to WT. See also Figure S3 and Figure S4.

in cortical neurons, CP is expressed in glia (Klomp et al., 1996). Coimmunoprecipitation of CP by anti-ferroportin was slightly but significantly increased in APP$^{-/-}$ brain tissue (Figures S4D and S4E), possibly due to loss of APP competition for ferroportin interaction. Therefore, ferroportin divides its interactions between APP and CP in the brain.

However, unlike APP695α (Figure 3B and Figure 4A), CP (2 μM) induced no significant increase in ^{59}Fe efflux when added to primary neurons or HEK293T cells (data not shown), consistent with previous observations that the ability of CP to stabilize ferroportin was cell type specific and probably limited to cells that express CP (De Domenico et al., 2007).

Consistent with APP ferroxidase activity being protective, the LD_{50} for Fe^{2+} toxicity was 10-fold higher for primary neurons in culture from WT (2001 μM) compared to those from APP$^{-/-}$ mice (234 μM, Figure 4F). However, domains and posttranslational modifications outside of the ferroxidase domain can promote protection against oxidative damage (Furukawa et al., 1996). To appraise the contribution of APP ferroxidase activity to neuroprotection against non-iron oxidative injuries, we studied the effects of APP695 compared to FD1$^{(E14N)}$-APP695 in protecting primary neurons from oxidative stress induced by glutamate excitotoxicity, where sAPPα prevents intracellular Ca^{2+} rise (Furukawa et al., 1996; Mattson et al., 1993). Whereas APP695 significantly prevented glutamate toxicity under these conditions, the ferroxidase mutant did not (Figure S3E). Although this result raises the hypothesis that some previously reported neuroprotective effects of APP may reflect ferroxidase activity, this is not surprising because the presence of labile iron exacerbates all forms of reactive oxygen species damage (through Fenton chemistry), and therefore the ability of the APP ferroxidase domain to minimize labile iron is likely to be protective to some extent against oxidative stress from any origin. We therefore tested whether APP protects the intact brain from toxicity induced by excess iron exposure.

APP Prevents Iron Accumulation and Oxidative Stress In Vivo

Aceruloplasminemic patients and CP knockout mice exhibit marked age-related iron accumulation in liver, pancreas, and brain astrocytes (Harris et al., 1995; Patel et al., 2002) but not cortical neurons (Gonzalez-Cuyar et al., 2008; Jeong and David, 2006; Patel et al., 2002). To test whether APP deficiency would cause a similar vulnerability, 12-month-old APP$^{-/-}$ mice were compared to WT age-matched controls fed a normal or high-iron diet for 8 days. Consistent with our cell culture findings (Figure 3 and Figure 4), APP$^{-/-}$ mice fed a normal diet had significantly more total iron in brain (+26%), liver (+31%), and kidney (+15%) tissue than age-matched controls (Figure 5A; Table S1). After challenge with the high-iron diet, WT mice had no significant change in tissue iron levels. In contrast, APP$^{-/-}$ mice accumulated significantly more iron in brain (+13%) and particularly liver (+90%) than APP$^{-/-}$ mice on a normal diet (Figure 5A). Ferritin levels were also increased in brain and liver

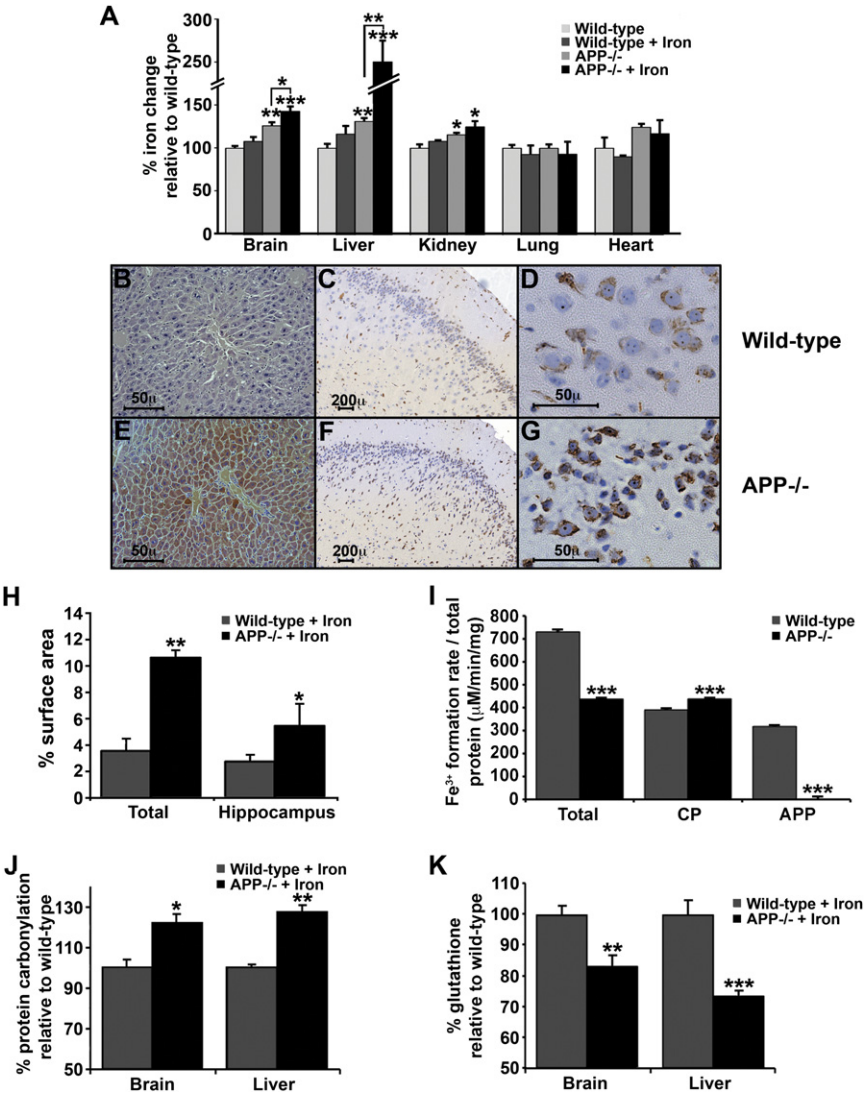

Figure 5. Dietary Iron Challenge Increases Tissue Iron in APP$^{-/-}$ but Not Normal Mice

(A) Twelve-month-old APP$^{-/-}$ mice accumulate iron within brain (~125%), liver (~130%), and kidney (~115%) tissue compared to WT matched controls. Iron levels were further increased in brain (~140%) and liver (~250%) of APP$^{-/-}$ mice fed a high iron diet for 8 days, which did not alter iron levels in WT matched controls.

(B–G) Labile redox-active iron detected by modified Perl's staining in hepatocytes (B and E) and cortical neurons (C, D, F, and G) from APP$^{-/-}$ (E–G) and WT matched controls (B–D) fed a high iron diet.

(H) Computer-assisted quantification of modified Perl's-stained surface area of brain sections from mice fed on a high iron diet (n = 4 mice, average of 3 sections each) indicates that APP$^{-/-}$ mice have significantly more redox-active iron-positive cells per hemisphere, and in the hippocampus, compared to WT.

(I) Ferroxidase activity in brain from APP$^{-/-}$ mice is decreased compared to WT matched controls. CP activity is determined after treatment of the tissue with Zn^{2+} to inhibit the activity of APP. APP activity is determined after treatment of the tissue with NaN_3 to inhibit the activity of CP.

(J–K) In accord with increased redox-active iron in liver and brain from APP$^{-/-}$ mice, significantly increased protein carbonylation occurs in APP$^{-/-}$ mice fed on a high iron diet (J) and decreased glutathione in APP$^{-/-}$ ± high iron diet (K).

Data are means ± SEM, n = 4, * = $p < 0.05$, ** = $p < 0.01$, *** = $p < 0.001$. (A) analyzed by ANOVA + Dunnet's test compared to WT, (H)–(K) by two-tailed t tests. See also Figure S4 and Table S1.

tissue from APP$^{-/-}$ mice on the high iron diet (data not shown) consistent with increased iron content. Iron supplementation did not affect the tissue levels of other metals (Table S1).

We examined the livers and cortex of APP$^{-/-}$ and WT mice with a modified Perl's histological stain, which utilizes intracellular Fe^{2+} to generate H_2O_2 (Gonzalez-Cuyar et al., 2008; Smith et al., 1997). This revealed elevated hepatocytic Fe^{2+} (Figures 5B and 5E) and intraneuronal Fe^{2+} (Figures 5C, 5D, and 5F–5H) of APP$^{-/-}$ mice compared to WT matched controls both fed iron. Fe^{2+} accumulation in the brain was confined to neocortical and hippocampal neurons (Figure 5H), while sparing microglia and astrocytes that are known to express CP (Gonzalez-Cuyar et al., 2008; Harris et al., 1995; Patel et al., 2002). Assay of tissue ferroxidase activity revealed a significant ~40% decrease in APP$^{-/-}$ brain (Figure 5I). NaN_3 inhibition of CP activity in WT brain tissue revealed ~40% residual activity and the complete loss of ferroxidase activity in the brains of APP$^{-/-}$ mice (Figure 5I). These data are consistent with APP acting as a neuronal ferroxidase. Suppression of APP activity in WT brain tissue with Zn^{2+} revealed ~60% activity, consistent with residual CP ferroxidase activity, and was slightly increased in APP$^{-/-}$ mice (Figure 5I), perhaps reflecting homeostatic compensation. There were no conspicuous changes in ferroportin or CP levels in liver and brain samples from APP$^{-/-}$ mice on a normal or iron-supplemented diet (Figure S4F).

The constitutive abundance of APP in WT liver was found to be similar to that of CP (Figure S4G). Therefore, the increase in liver iron in APP$^{-/-}$ mice was consistent with a major loss in the total ferroxidase complement of the tissue. Conversely, APP$^{-/-}$ heart and lung tissue did not show elevated iron levels even with dietary iron challenge, consistent with these organs having the lowest constitutive levels of APP (Figure S4G) and expressing alternative iron-export ferroxidases, CP (Figure S4G), and hephaestin (Qian et al., 2007). Similarly, APP levels in astrocytes are much lower than in neurons (Gray and Patel, 1993; Mita et al., 1989; Rohan de Silva et al., 1997), and probably too low to prevent iron accumulation in CP$^{-/-}$ astrocytes. Cortical neurons have no redundancy in their export ferroxidases and therefore

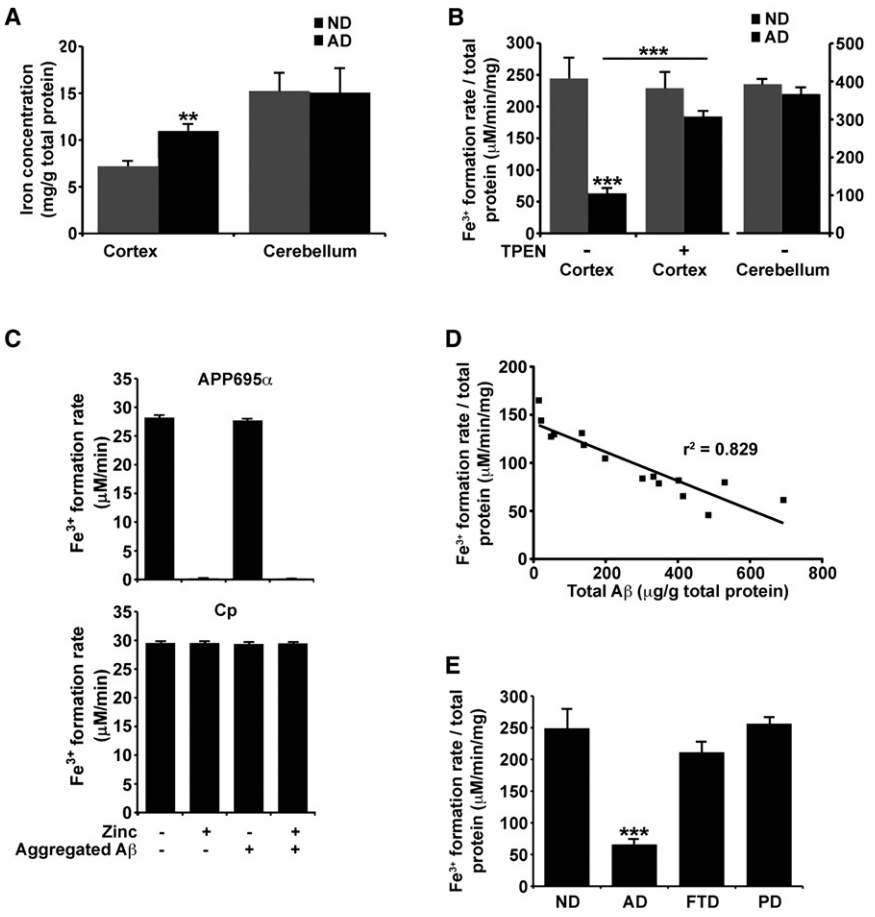

Figure 6. Decreased Cortical APP Ferroxidase Activity in Alzheimer's Disease

(A) AD cortical tissue accumulates iron compared to age-matched nondemented (ND) samples. Iron levels were not changed in pathologically unaffected cerebellum from the same subjects.

(B) APP-specific ferroxidase activity is decreased in AD cortical tissue (~75%) but not in cerebellum, consistent with the pattern of iron accumulation in (A). Chelating Zn^{2+} from the tissue with TPEN restores the APP ferroxidase activity in AD sample to levels comparable to ND cortex.

(C) Both free Zn^{2+}, as well as Zn^{2+} dissociating from washed Zn^{2+}:$A\beta_{1-42}$ aggregates, inhibit APP695α ferroxidase activity but not CP activity.

(D) Decrease in APP-specific ferroxidase activity correlates with increased Aβ content in AD cortical tissue ($p < 0.0001$, $r^2 = 0.829$).

(E) APP ferroxidase activity is not changed in cortical tissue from non-β-amyloid burdened neurodegenerative diseases such as Frontotemporal dementia and Parkinson's disease.

(A–C and E) Data are means ± SEM, n = 8, ** = $p < 0.01$, *** = $p < 0.001$ by two-tailed t tests.

See also Figure S1, Figure S5, and Table S2.

accumulate iron in the absence of APP (Figures 5F–5H). The likelihood that APP is the unique ferroxidase of cortical neurons is supported by the lack of iron increase in the cortical neurons of $CP^{-/-}$ mice even at an age (24 months) when there is a marked increase in iron in other cells (Jeong and David, 2006; Patel et al., 2002).

Increased Fe^{2+} generates oxidative stress, and indeed the Fe^{2+} increase detected in iron-fed $APP^{-/-}$ mice was accompanied by increased protein carbonylation (indicative of hydroxyl radical damage, Figure 5J) and decreased glutathione levels (Figure 5K), signifying depleted antioxidant reserves. Despite these signs of stress, stereological counting revealed no significant neuronal loss within the brain in iron-fed mice (data not shown). A more protracted period of iron exposure, or higher doses, may be needed to overcome survival defenses. The observation that iron enters the brain neurons of iron-fed $APP^{-/-}$ mice (Figure 5) also indicates either that APP is a component of the blood-brain barrier or that prandial iron normally transits the blood-brain barrier to neurons where it is then exported in an APP-dependent manner.

APP Ferroxidase Activity Is Inhibited by Zinc in Alzheimer's Disease

We explored whether a failure of APP ferroxidase activity could contribute to the elevated cortical iron that characterizes AD pathology. Elevated iron and ferritin are prominent within the vicinity of amyloid plaques in both humans (Grundke-Iqbal et al., 1990; Lovell et al., 1998; Robinson et al., 1995) and APP transgenic mice (El Tannir El Tayara et al., 2006; Falangola et al., 2005; Jack et al., 2005). We indeed found an ~45% increase in iron in postmortem AD cortical tissue (Brodmann area 46) but no change in pathologically unaffected cerebellum from the same patients (Figure 6A). This matched a 75% ($p < 0.001$) decrease in APP ferroxidase activity in the same AD cortical samples compared to the nondemented age-matched samples, with no difference in cerebellar tissue activities (Figure 6B). The ferroxidase activities were confirmed to be APP by immunodepletion experiments (Figure S5A).

The loss of APP ferroxidase activity in AD cortex was not due to decreased levels of APP (Figure S5B). Therefore, a factor in AD cortex appears to inhibit APP. Zn^{2+} is the only identified inhibitor of APP ferroxidase activity (Figure 2A), but total zinc levels were not significantly elevated in the AD cortical samples (Figure S5C). However, Zn^{2+} characteristically accumulates in extracellular amyloid in AD (Lovell et al., 1998; Religa et al., 2006; Suh et al., 2000), which is too small a volume fraction to elevate total tissue zinc levels until the disease is advanced (Religa et al., 2006). Indeed, treatment of the AD cortical samples with the Zn^{2+}-selective chelator TPEN restored APP ferroxidase activity to levels not significantly different from nondemented samples (Figure 6B), confirming that APP is inhibited by Zn^{2+} in AD tissue. TPEN did not significantly change ferroxidase activity in nondemented cortical samples (Figure 6B), indicating that Zn^{2+} is not inhibiting APP in normal tissue. To confirm that the APP ferroxidase activity in AD is being inhibited by Zn^{2+}, we titrated

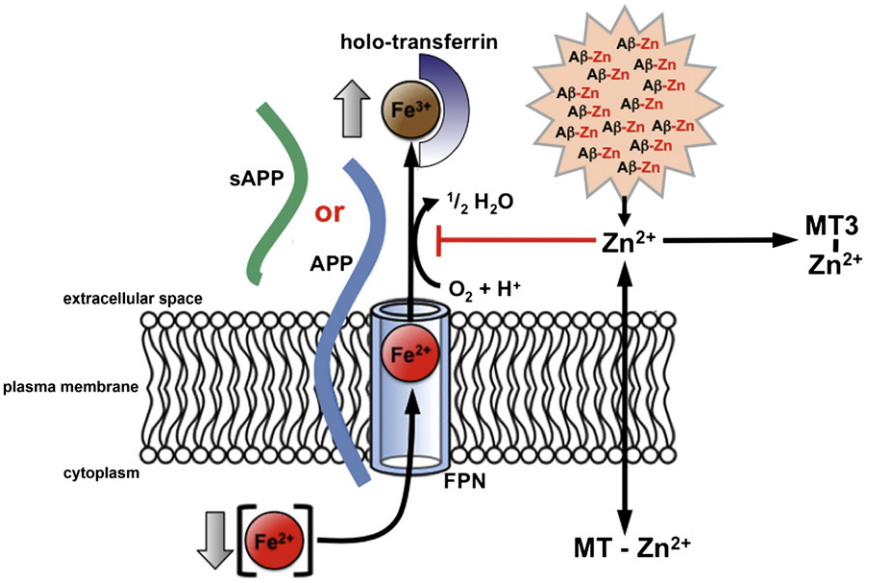

Figure 7. Model for the Role of APP in Cellular Iron Export and Its Inhibition in Alzheimer's Disease

FPN transports Fe^{2+} from the cytosol across the plasma membrane. Fe^{2+} is then converted to Fe^{3+} by a membrane-bound or soluble ferroxidase such as CP or APP (shown). The absence of the ferroxidase results in decreased iron release into the extracellular space, as Fe^{2+} is unable to be converted into Fe^{3+}. APP ferroxidase is inhibited by extracellular Zn^{2+} (Figure 2A and Figure 6B), which can exchange from $A\beta:Zn^{2+}$ aggregates (Figure 6D). Free Zn^{2+} is normally buffered by the presence of ligands such as metallothioneins (including metallothionein III in the extracellular space), which are lost in AD (Uchida et al., 1991). Loss of metallothioneins and other Zn^{2+} buffers may lie upstream in amyloid pathology, APP ferroxidase inhibition, and neuronal iron accumulation in AD. See also Figure S6.

additional Zn^{2+} into samples that had been treated with 20 μM TPEN (Figure S5D). Whereas Zn^{2+} concentrations of ≥20 μM were required to suppress APP ferroxidase activity in normal tissue under these conditions, far lower Zn^{2+} concentrations (≥2 μM) suppressed activity in AD samples (IC_{50} for normal tissue = 22.6 μM, IC_{50} for AD = 10.2 μM, Figure S5D). Together these data indicate that although there is no clear elevation in total zinc in AD tissue, there is a greater fraction of exchangeable Zn^{2+}, which is inhibiting APP ferroxidase.

Is the Zn^{2+} trapped in extracellular Aβ deposits sufficiently exchangeable to be the source of Zn^{2+} that inhibits APP ferroxidase in AD tissue? To test this we prepared washed (no free Zn^{2+}) synthetic $A\beta:Zn^{2+}$ precipitates and found that they indeed inhibited APP695α activity as efficiently as free Zn^{2+} in solution, whereas Aβ alone had no effect (Figure 6C). Therefore, Aβ traps Zn^{2+} but can readily exchange the Zn^{2+} with APP. Neither free Zn^{2+} nor $A\beta:Zn^{2+}$ complexes inhibited CP activity (Figure 6C).

Consistent with Aβ presenting Zn^{2+} to suppress APP ferroxidase activity in the brain, there was a significant negative correlation between Aβ burden and APP ferroxidase activity in a series of AD ($p < 0.0001$, Figure 6D) and APP transgenic (Tg2576, Figures S5E and S5F) cortical samples. However, APP ferroxidase activity was not diminished in cortical tissue from Frontotemporal dementia or Parkinson's disease (Figure 6E) that lacked amyloid pathology (Table S2), or from Tg2576 mice at an age prior to amyloid pathology (Figures S5E and S5F).

DISCUSSION

Our findings identify APP as a functional ferroxidase similar to CP. Both full-length and soluble APP species were found to have major interactions with ferroportin to facilitate iron export from certain cells including neurons (Figure 7). CP similarly exists in GPI-anchored and -soluble forms, with the purpose of separate pools remaining uncertain, although activity at a distance from the cell of origin is likely. While the ferroxidase function of APP is compatible with IRE-regulated translation (Rogers et al., 2002), the relationship between iron-load and APP processing remains to be elucidated, although we note a prior report that exogenous iron promotes α-cleavage in cell culture (Bodovitz et al., 1995). APP therefore plays an important role in preventing iron-mediated oxidative stress through separate domains: an HO-inhibitory domain (Figure 1A) that prevents the release of Fe^{2+} from heme (Takahashi et al., 2000) and, here, a separate ferroxidase domain. The ferroxidase activity of the APP is unique among its protein family and, like ferritin, correlates with the presence of the mRNA IRE motif, which is not present in APLP1 and APLP2 (Figure S6). The ferroxidase center of APP resides in the REXXE consensus motif of the E2 domain, with a remote potentiation domain within the GFD of E1 (Figure 1 and Figure 2). This potentiation by heterologous components is reminiscent of the augmentation of H-ferritin ferroxidase activity by L-ferritin, where the active site is on H-ferritin yet heteropolymers of H and L subunits have a higher ferroxidase activity per H subunit than H homopolymers (Yang et al., 1998).

CP and APP may be backup ferroxidase activities in tissues where they are colocated (Figures S4E and S4G) or in glia that express both APP and CP. The purpose behind such apparent redundancy in some cells is yet unclear. But as neurons lack CP, APP may be the sole iron-export ferroxidase of neurons. Our findings indicate that inhibition of APP ferroxidase activity may contribute to neuronal iron accumulation in AD cortex. Elevated brain iron is a complication of aging (Bartzokis et al., 1994a; De Domenico et al., 2008; Hallgren and Sourander, 1958; Maynard et al., 2002) and is a feature of several neurodegenerative disorders (Zecca et al., 2004). Failure of ferroxidases CP (Harris et al., 1995), ferritin (Chinnery et al., 2007), and frataxin (Mantovan et al., 2006) cause various neurodegenerative diseases, and it is intriguing that here another systemically expressed ferroxidase, APP, is linked to a major brain disease, AD. The elevation of brain iron in AD affects the parenchyma (Bartzokis et al., 1994b; Honda et al., 2005; Smith et al., 1997)

but is particularly conspicuous in the dystrophic neurites of amyloid plaques (Grundke-Iqbal et al., 1990; Lovell et al., 1998; Robinson et al., 1995) where its MRI signal in AD correlates with dementia severity (Ding et al., 2009).

Our data indicate a mechanism by which amyloid pathology could disrupt local iron homeostasis. We found that APP ferroxidase activity is inhibited by a tissue source of Zn^{2+} in AD cortical tissue (Figure 6B). In AD cortex, Aβ binds Zn^{2+} to achieve pathological concentrations (~1 mM) in plaques (Dong et al., 2003; Lovell et al., 1998; Opazo et al., 2002) and seems a possible reservoir for APP inhibition. Supporting this possibility, Aβ readily transfers Zn^{2+} to inhibit APP ferroxidase activity (Figure 6C), exchangeable Zn^{2+} (as measured by APP inhibition) is increased in AD tissue (Figure S5D), and Aβ burden inversely correlates with APP ferroxidase activity (Figure 6D). Additionally, Zn^{2+} buffering appears far more limited in AD cortex than nondemented tissue (Figure S5D), which could be consistent with loss of metallothionein III (Uchida et al., 1991) that is released into the synaptic vicinity by astrocytes and prevents metal ion transfer to Aβ (Meloni et al., 2008). Alternatively, oxidation, which is marked in AD tissue, may prevent metallothioneins from binding Zn^{2+} (Hao and Maret, 2005). As Zn^{2+} induces Aβ aggregation (Bush et al., 1994; Lee et al., 2002), we hypothesize that loss of Zn^{2+} buffering may be an upstream lesion for both amyloid pathology and APP ferroxidase inhibition (Figure 7).

APP is another elevated component of dystrophic neurites within plaque (Cras et al., 1991) where, as noted above, it colocates with high iron concentrations. We hypothesize that in neuritic pathology, elevated iron summons further APP production (Rogers et al., 2002), but the APP generated to export iron becomes inhibited by elevated extracellular Zn^{2+} dissociating from Aβ (Figure 7). This underscores the buffering of Zn^{2+} as a therapeutic strategy for AD and could explain some activities of Zn^{2+} ionophores (clioquinol and PBT2) that have shown potent efficacy in preclinical APP transgenic models of AD (Adlard et al., 2008; Cherny et al., 2001) and significantly improved cognition in phase 2 AD clinical trials (Faux et al., 2010; Lannfelt et al., 2008; Ritchie et al., 2003).

The ferroxidase and iron-trafficking properties of APP indicate an important biological activity for a protein whose complex processing has been extensively studied but which has lacked a conspicuous purpose. These data indicate that some neurotrophic properties of APP and its fragments (Rossjohn et al., 1999) could be mediated by iron regulation.

EXPERIMENTAL PROCEDURES

Human

All human tissue cases were obtained from the Victorian Brain Bank Network. Whole brains were stored at −80°C until required. Cortical tissue from nondemented controls, AD, Parkinson's disease, and Frontotemporal dementia were all taken from Brodmann's area 46. Cerebellum tissue was also used from nondemented controls and AD patients. For Aβ analysis, western blots were carried out on total brain homogenates. Ferroxidase activity was tested by transferrin ferroxidase assay on PBS + 1% Triton X-100 (PBST) extracted homogenates.

Biotin Labeling of APP695α

Sulfo-NHS-SS-Biotin (Thermo Scientific) was added to APP695α in 20-fold excess and incubated at room temperature for 1 hr in phosphate-buffered saline (PBS). Removal of nonreacted sulfo-NHS-SS-Biotin was by gel filtration using a Zeba Desalt spin column (Thermo Scientific).

Aβ Preparation

For aggregation studies, 100 μM $Aβ_{1–42}$ was incubated ± 200 μM $ZnCl_2$ for 16 hr to form precipitates as previously reported (Bush et al., 1994). Insoluble $Aβ_{1–42}$ was then centrifuged at 40,000 g for 10 min and the pellet repeatedly washed in PBS. Aggregated $Aβ_{1–42}$ ± Zn was then added to the Tf ferroxidase assay (described below) at a final concentration of 10 μM $Aβ_{1–42}$ and compared to controls including freshly prepared nonaggregated 10 μM $Aβ_{1–42}$.

Transferrin Ferroxidase Assay

The assay was based upon established procedures (Bakker and Boyer, 1986), utilizing the spectroscopic change in apo-transferrin when loaded with Fe^{3+}. K_m and V_{max} values and curve-fitting were calculated by GraphPad Prism v 5.0. In a cuvette was added (in order): 100 μl ddH_2O, 200 μl HBS buffer (150 mM NaCl, 50 mM HEPES), pH 7.2, 200 μl of 275 μM apo-transferrin, 100 μl of sample (200 nM recombinant protein or 30 μg total tissue homogenate) and 400 μl of 275 μM ferrous ammonium sulfate $(NH_4)_2Fe(SO_4)_2$. For studies of pH-dependence, the buffers (50 mM) were: pH 5 sodium acetate, pH 5.5–6.5 MES, pH 7.0–9.0 Tris. The mixture was incubated for 5 min at 37°C with agitation, and absorbance read at 460 nm. Extinction coefficient of diferric transferrin is 4.56 mM^{-1}.

Immunoprecipitation

HEK293T cells (±3 hr preincubation with 2 μM biotin-APP695α), or brain homogenate, was extracted into PBST. Human brain membrane homogenates were extracted in PBS and then sodium carbonate (pH 11). Protein content was then determined by BCA. One hundred micrograms of the sample was then precleared for nonspecific binding with protein G agarose beads for 1 hr at 4°C. The sample was then incubated with capture antibody (rabbit anti-ferroportin, 1:200, Lifespan Biosciences), mouse anti-N-term APP (22C11), rabbit anti-CP, or mouse anti-APLP2 (1:1000, R&D systems) for 1 hr (4°C) before adding fresh equilibrated protein G agarose beads and mixed for a further 2–3 hr (4°C). Protein G agarose beads were then washed in PBST and bound proteins were eluted with SDS-PAGE loading buffer. The bound and unbound proteins were separated on 4%–20% PAGE (Bis-Tris, Invitrogen) and visualized by western analysis with a detection antibody: mouse anti-N-term APP, mouse anti-Aβ domain of APP (1:500, WO2), rabbit anti-C-term APP (1:10,000, Chemicon), rabbit anti-ferroportin, or, in the case of biotin-labeled studies, streptavidin crosslinked to horseradish peroxidase (HRP, 1:15,000, Invitrogen).

Histochemical Detection of Iron by Perl's Staining

For direct visualization of redox-active Fe^{2+} in whole brain hemisphere and liver paraffin-embedded sections, a modified Perl's technique was used, as previously described (Gonzalez-Cuyar et al., 2008; Smith et al., 1997). The number of iron-positive structures was quantified using color selection to separate cells from background. Deparaffinized and rehydrated tissue sections (7 μm) were incubated at 37°C for 1 hr in 7% potassium ferrocyanide with aqueous hydrochloric acid (3%) and subsequently incubated in 0.75 mg/ml 3,3′-diaminobenzidine and 0.015% H_2O_2 for 5–10 min. When required, sections were counterstained in Mayer's hematoxylin for 2 min and washed in Scott's tap water before mounting. For brain, the number of iron-positive structures was quantified using color selection to separate cells from background as described in Extended Experimental Procedures.

SUPPLEMENTAL INFORMATION

Supplemental Information includes Extended Experimental Procedures, three figures, and one table and can be found with this article online at doi:10.1016/j.cell.2010.08.014.

ACKNOWLEDGMENTS

This work was supported by funds from the National Institute on Aging (1RO1AG12686), the Australian Research Council, the Australian National

Health & Medical Research Council (NHMRC), Operational Infrastructure Support Victorian State Government, and the Alzheimer's Association. The Victorian Brain Bank Network is supported by The University of Melbourne, The Mental Health Research Institute, The Alfred Hospital, and the Victorian Forensic Institute of Medicine and funded by Neurosciences Australia and the NHMRC. We thank Gerd Multhaup for helpful comments and for providing APP reagents for pilot studies, Paul Adlard for human tissue samples, and Wilma Wasco for the APLP2 construct. C.L.M., R.E.T., K.J.B., and A.I.B. are shareholders, paid consultants, and advisory board members of Prana Biotechnology Ltd. A.I.B. is a shareholder of Cogstate Ltd and Eucalyptus Biosciences Pty Ltd. M.A.C. is a shareholder in Prana Biotechnology Ltd.

Received: February 22, 2010
Revised: May 25, 2010
Accepted: July 23, 2010
Published online: September 2, 2010

REFERENCES

Adlard, P.A., Cherny, R.A., Finkelstein, D.I., Gautier, E., Robb, E., Cortes, M., Volitakis, I., Liu, X., Smith, J.P., Perez, K., et al. (2008). Rapid restoration of cognition in Alzheimer's transgenic mice with 8-hydroxy quinoline analogs is associated with decreased interstitial Abeta. Neuron *59*, 43–55.

Bakker, G.R., and Boyer, R.F. (1986). Iron incorporation into apoferritin. The role of apoferritin as a ferroxidase. J. Biol. Chem. *261*, 13182–13185.

Bartzokis, G., and Tishler, T.A. (2000). MRI evaluation of basal ganglia ferritin iron and neurotoxicity in Alzheimer's and Huntingon's disease. Cell. Mol. Biol. (Noisy-le-grand) *46*, 821–833.

Bartzokis, G., Mintz, J., Sultzer, D., Marx, P., Herzberg, J.S., Phelan, C.K., and Marder, S.R. (1994a). In vivo MR evaluation of age-related increases in brain iron. AJNR Am. J. Neuroradiol. *15*, 1129–1138.

Bartzokis, G., Sultzer, D., Mintz, J., Holt, L.E., Marx, P., Phelan, C.K., and Marder, S.R. (1994b). In vivo evaluation of brain iron in Alzheimer's disease and normal subjects using MRI. Biol. Psychiatry *35*, 480–487.

Bodovitz, S., Falduto, M.T., Frail, D.E., and Klein, W.L. (1995). Iron levels modulate alpha-secretase cleavage of amyloid precursor protein. J. Neurochem. *64*, 307–315.

Bush, A.I., Pettingell, W.H., Multhaup, G., d Paradis, M., Vonsattel, J.P., Gusella, J.F., Beyreuther, K., Masters, C.L., and Tanzi, R.E. (1994). Rapid induction of Alzheimer A beta amyloid formation by zinc. Science *265*, 1464–1467.

Cherny, R.A., Legg, J.T., McLean, C.A., Fairlie, D., Huang, X., Atwood, C.S., Beyreuther, K., Tanzi, R.E., Masters, C.L., and Bush, A.I. (1999). Aqueous dissolution of Alzheimer's disease Aß amyloid deposits by biometal depletion. J. Biol. Chem. *274*, 23223–23228.

Cherny, R.A., Atwood, C.S., Xilinas, M.E., Gray, D.N., Jones, W.D., McLean, C.A., Barnham, K.J., Volitakis, I., Fraser, F.W., Kim, Y., et al. (2001). Treatment with a copper-zinc chelator markedly and rapidly inhibits beta-amyloid accumulation in Alzheimer's disease transgenic mice. Neuron *30*, 665–676.

Chinnery, P.F., Crompton, D.E., Birchall, D., Jackson, M.J., Coulthard, A., Lombes, A., Quinn, N., Wills, A., Fletcher, N., Mottershead, J.P., et al. (2007). Clinical features and natural history of neuroferritinopathy caused by the FTL1 460InsA mutation. Brain *130*, 110–119.

Cras, P., Kawai, M., Lowery, D., Gonzalez-DeWhitt, P., Greenberg, B., and Perry, G. (1991). Senile plaque neurites in Alzheimer disease accumulate amyloid precursor protein. Proc. Natl. Acad. Sci. USA *88*, 7552–7556.

De Domenico, I., Ward, D.M., di Patti, M.C., Jeong, S.Y., David, S., Musci, G., and Kaplan, J. (2007). Ferroxidase activity is required for the stability of cell surface ferroportin in cells expressing GPI-ceruloplasmin. EMBO J. *26*, 2823–2831.

De Domenico, I., Nemeth, E., Nelson, J.M., Phillips, J.D., Ajioka, R.S., Kay, M.S., Kushner, J.P., Ganz, T., Ward, D.M., and Kaplan, J. (2008). The hepcidin-binding site on ferroportin is evolutionarily conserved. Cell Metab. *8*, 146–156.

Ding, B., Chen, K.M., Ling, H.W., Sun, F., Li, X., Wan, T., Chai, W.M., Zhang, H., Zhan, Y., and Guan, Y.J. (2009). Correlation of iron in the hippocampus with MMSE in patients with Alzheimer's disease. J. Magn. Reson. Imaging *29*, 793–798.

Dong, J., Atwood, C.S., Anderson, V.E., Siedlak, S.L., Smith, M.A., Perry, G., and Carey, P.R. (2003). Metal binding and oxidation of amyloid-beta within isolated senile plaque cores: Raman microscopic evidence. Biochemistry *42*, 2768–2773.

El Tannir El Tayara, N., Delatour, B., Le Cudennec, C., Guegan, M., Volk, A., and Dhenain, M. (2006). Age-related evolution of amyloid burden, iron load, and MR relaxation times in a transgenic mouse model of Alzheimer's disease. Neurobiol. Dis. *22*, 199–208.

Falangola, M.F., Lee, S.P., Nixon, R.A., Duff, K., and Helpern, J.A. (2005). Histological co-localization of iron in Abeta plaques of PS/APP transgenic mice. Neurochem. Res. *30*, 201–205.

Faux, N.G., Ritchie, C.W., Gunn, A., Rembach, A., Tsatsanis, A., Bedo, J., Harrison, J., Lannfelt, L., Blennow, K., Zetterberg, H., et al. (2010). PBT2 rapidly improves cognition in Alzheimer's disease: additional phase II analyses. J. Alzheimers Dis. *20*, 509–516.

Furukawa, K., Sopher, B.L., Rydel, R.E., Begley, J.G., Pham, D.G., Martin, G.M., Fox, M., and Mattson, M.P. (1996). Increased activity-regulating and neuroprotective efficacy of alpha-secretase-derived secreted amyloid precursor protein conferred by a C-terminal heparin-binding domain. J. Neurochem. *67*, 1882–1896.

Gonzalez-Cuyar, L.F., Perry, G., Miyajima, H., Atwood, C.S., Riveros-Angel, M., Lyons, P.F., Siedlak, S.L., Smith, M.A., and Castellani, R.J. (2008). Redox active iron accumulation in aceruloplasminemia. Neuropathology *28*, 466–471.

Gray, C.W., and Patel, A.J. (1993). Induction of beta-amyloid precursor protein isoform mRNAs by bFGF in astrocytes. Neuroreport *4*, 811–814.

Grundke-Iqbal, I., Fleming, J., Tung, Y.C., Lassmann, H., Iqbal, K., and Joshi, J.G. (1990). Ferritin is a component of the neuritic (senile) plaque in Alzheimer dementia. Acta Neuropathol. *81*, 105–110.

Gutierrez, J.A., Yu, J., Rivera, S., and Wessling-Resnick, M. (1997). Functional expression cloning and characterization of SFT, a stimulator of Fe transport. J. Cell Biol. *139*, 895–905.

Hallgren, B., and Sourander, P. (1958). The effect of age on the non-haemin iron in the human brain. J. Neurochem. *3*, 41–51.

Hao, Q., and Maret, W. (2005). Imbalance between pro-oxidant and pro-antioxidant functions of zinc in disease. J. Alzheimers Dis. *8*, 161–170.

Harris, Z.L., Takahashi, Y., Miyajima, H., Serizawa, M., MacGillivray, R.T., and Gitlin, J.D. (1995). Aceruloplasminemia: molecular characterization of this disorder of iron metabolism. Proc. Natl. Acad. Sci. USA *92*, 2539–2543.

Honda, K., Smith, M.A., Zhu, X., Baus, D., Merrick, W.C., Tartakoff, A.M., Hattier, T., Harris, P.L., Siedlak, S.L., Fujioka, H., et al. (2005). Ribosomal RNA in Alzheimer disease is oxidized by bound redox-active iron. J. Biol. Chem. *280*, 20978–20986.

Jack, C.R., Jr., Wengenack, T.M., Reyes, D.A., Garwood, M., Curran, G.L., Borowski, B.J., Lin, J., Preboske, G.M., Holasek, S.S., Adriany, G., et al. (2005). In vivo magnetic resonance microimaging of individual amyloid plaques in Alzheimer's transgenic mice. J. Neurosci. *25*, 10041–10048.

Jeong, S.Y., and David, S. (2003). Glycosylphosphatidylinositol-anchored ceruloplasmin is required for iron efflux from cells in the central nervous system. J. Biol. Chem. *278*, 27144–27148.

Jeong, S.Y., and David, S. (2006). Age-related changes in iron homeostasis and cell death in the cerebellum of ceruloplasmin-deficient mice. J. Neurosci. *26*, 9810–9819.

Klausner, R.D., Rouault, T.A., and Harford, J.B. (1993). Regulating the fate of mRNA: The control of cellular iron metabolism. Cell *72*, 19–28.

Klomp, L.W., Farhangrazi, Z.S., Dugan, L.L., and Gitlin, J.D. (1996). Ceruloplasmin gene expression in the murine central nervous system. J. Clin. Invest. *98*, 207–215.

Lannfelt, L., Blennow, K., Zetterberg, H., Batsman, S., Ames, D., Harrison, J., Masters, C.L., Targum, S., Bush, A.I., Murdoch, R., et al. (2008). Safety,

efficacy, and biomarker findings of PBT2 in targeting Abeta as a modifying therapy for Alzheimer's disease: a phase IIa, double-blind, randomised, placebo-controlled trial. Lancet Neurol. *7*, 779–786.

Lawson, D.M., Artymiuk, P.J., Yewdall, S.J., Smith, J.M., Livingstone, J.C., Treffry, A., Luzzago, A., Levi, S., Arosio, P., Cesareni, G., et al. (1991). Solving the structure of human H ferritin by genetically engineering intermolecular crystal contacts. Nature *349*, 541–544.

Lawson, D.M., Treffry, A., Artymiuk, P.J., Harrison, P.M., Yewdall, S.J., Luzzago, A., Cesareni, G., Levi, S., and Arosio, P. (1989). Identification of the ferroxidase centre in ferritin. FEBS Lett. *254*, 207–210.

Lee, J.-Y., Cole, T.B., Palmiter, R.D., Suh, S.W., and Koh, J.-Y. (2002). Contribution by synaptic zinc to the gender-disparate plaque formation in human Swedish mutant APP transgenic mice. Proc. Natl. Acad. Sci. USA *99*, 7705–7710.

Lovell, M.A., Robertson, J.D., Teesdale, W.J., Campbell, J.L., and Markesbery, W.R. (1998). Copper, iron and zinc in Alzheimer's disease senile plaques. J. Neurol. Sci. *158*, 47–52.

Mantovan, M.C., Martinuzzi, A., Squarzanti, F., Bolla, A., Silvestri, I., Liessi, G., Macchi, C., Ruzza, G., Trevisan, C.P., and Angelini, C. (2006). Exploring mental status in Friedreich's ataxia: a combined neuropsychological, behavioral and neuroimaging study. Eur. J. Neurol. *13*, 827–835.

Mattson, M.P., Cheng, B., Culwell, A.R., Esch, F.S., Lieberburg, I., and Rydel, R.E. (1993). Evidence for excitoprotective and intraneuronal calcium-regulating roles for secreted forms of the β-amyloid precursor protein. Neuron *10*, 243–254.

Maynard, C.J., Cappai, R., Volitakis, I., Cherny, R.A., White, A.R., Beyreuther, K., Masters, C.L., Bush, A.I., and Li, Q.X. (2002). Overexpression of Alzheimer's disease amyloid-beta opposes the age-dependent elevations of brain copper and iron. J. Biol. Chem. *277*, 44670–44676.

Meloni, G., Sonois, V., Delaine, T., Guilloreau, L., Gillet, A., Teissie, J., Faller, P., and Vasak, M. (2008). Metal swap between Zn7-metallothionein-3 and amyloid-beta-Cu protects against amyloid-beta toxicity. Nat. Chem. Biol. *4*, 366–372.

Miller, L.M., Wang, Q., Telivala, T.P., Smith, R.J., Lanzirotti, A., and Miklossy, J. (2006). Synchrotron-based infrared and X-ray imaging shows focalized accumulation of Cu and Zn co-localized with beta-amyloid deposits in Alzheimer's disease. J. Struct. Biol. *155*, 30–37.

Mita, S., Schon, E.A., and Herbert, J. (1989). Widespread expression of amyloid beta-protein precursor gene in rat brain. Am. J. Pathol. *134*, 1253–1261.

Ninomiya, H., Roch, J.M., Sundsmo, M.P., Otero, D.A., and Saitoh, T. (1993). Amino acid sequence RERMS represents the active domain of amyloid beta/A4 protein precursor that promotes fibroblast growth. J. Cell Biol. *121*, 879–886.

Opazo, C., Huang, X., Cherny, R., Moir, R., Roher, A., White, A., Cappai, R., Masters, C., Tanzi, R., Inestrosa, N., et al. (2002). Metalloenzyme-like activity of Alzheimer's disease β-amyloid: Cu-dependent catalytic conversion of dopamine, cholesterol and biological reducing agents to neurotoxic H_2O_2. J. Biol. Chem. *277*, 40302–40308.

Osaki, S. (1966). Kinetic studies of ferrous ion oxidation with crystalline human ferroxidase (ceruloplasmin). J. Biol. Chem. *241*, 5053–5059.

Patel, B.N., Dunn, R.J., Jeong, S.Y., Zhu, Q., Julien, J.P., and David, S. (2002). Ceruloplasmin regulates iron levels in the CNS and prevents free radical injury. J. Neurosci. *22*, 6578–6586.

Qian, Z.M., Chang, Y.Z., Leung, G., Du, J.R., Zhu, L., Wang, Q., Niu, L., Xu, Y.J., Yang, L., Ho, K.P., et al. (2007). Expression of ferroportin1, hephaestin and ceruloplasmin in rat heart. Biochim. Biophys. Acta *1772*, 527–532.

Religa, D., Strozyk, D., Cherny, R.A., Volitakis, I., Haroutunian, V., Winblad, B., Naslund, J., and Bush, A.I. (2006). Elevated cortical zinc in Alzheimer disease. Neurology *67*, 69–75.

Ritchie, C.W., Bush, A.I., Mackinnon, A., Macfarlane, S., Mastwyk, M., MacGregor, L., Kiers, L., Cherny, R., Li, Q.X., Tammer, A., et al. (2003). Metal-protein attenuation with iodochlorhydroxyquin (clioquinol) targeting Abeta amyloid deposition and toxicity in Alzheimer disease: a pilot phase 2 clinical trial. Arch. Neurol. *60*, 1685–1691.

Robinson, S.R., Noone, D.F., Kril, J., and Halliday, G.M. (1995). Most amyloid plaques contain ferritin-rich cells. Alzheimer's Res. *1*, 191–196.

Rogers, J.T., Randall, J.D., Cahill, C.M., Eder, P.S., Huang, X., Gunshin, H., Leiter, L., McPhee, J., Sarang, S.S., Utsuki, T., et al. (2002). An iron-responsive element type II in the 5′-untranslated region of the Alzheimer's amyloid precursor protein transcript. J. Biol. Chem. *277*, 45518–45528.

Rohan de Silva, H.A., Jen, A., Wickenden, C., Jen, L.S., Wilkinson, S.L., and Patel, A.J. (1997). Cell-specific expression of beta-amyloid precursor protein isoform mRNAs and proteins in neurons and astrocytes. Brain Res. Mol. Brain Res. *47*, 147–156.

Rossjohn, J., Cappai, R., Feil, S.C., Henry, A., McKinstry, W.J., Galatis, D., Hesse, L., Multhaup, G., Beyreuther, K., Masters, C.L., et al. (1999). Crystal structure of the N-terminal, growth factor-like domain of Alzheimer amyloid precursor protein. Nat. Struct. Biol. *6*, 327–331.

Smith, M.A., Harris, P.L., Sayre, L.M., and Perry, G. (1997). Iron accumulation in Alzheimer disease is a source of redox-generated free radicals. Proc. Natl. Acad. Sci. USA *94*, 9866–9868.

Suh, S.W., Jensen, K.B., Jensen, M.S., Silva, D.S., Kesslak, P.J., Danscher, G., and Frederickson, C.J. (2000). Histochemically-reactive zinc in amyloid plaques, angiopathy, and degenerating neurons of Alzheimer's diseased brains. Brain Res. *852*, 274–278.

Takahashi, M., Dore, S., Ferris, C.D., Tomita, T., Sawa, A., Wolosker, H., Borchelt, D.R., Iwatsubo, T., Kim, S.H., Thinakaran, G., et al. (2000). Amyloid precursor proteins inhibit heme oxygenase activity and augment neurotoxicity in Alzheimer's disease. Neuron *28*, 461–473.

Toussaint, L., Bertrand, L., Hue, L., Crichton, R.R., and Declercq, J.P. (2007). High-resolution X-ray structures of human apoferritin H-chain mutants correlated with their activity and metal-binding sites. J. Mol. Biol. *365*, 440–452.

Uchida, Y., Takio, K., Titani, K., Ihara, Y., and Tomonaga, M. (1991). The growth-inhibitory factor that is deficient in the Alzheimer's disease brain is a 68-amino acid metallothionein-like protein. Neuron *7*, 337–347.

Visser, C.C., Voorwinden, L.H., Crommelin, D.J., Danhof, M., and de Boer, A.G. (2004). Characterization and modulation of the transferrin receptor on brain capillary endothelial cells. Pharm. Res. *21*, 761–769.

Wang, Y., and Ha, Y. (2004). The X-ray structure of an antiparallel dimer of the human amyloid precursor protein E2 domain. Mol. Cell *15*, 343–353.

Yamamoto, A., Shin, R.W., Hasegawa, K., Naiki, H., Sato, H., Yoshimasu, F., and Kitamoto, T. (2002). Iron (III) induces aggregation of hyperphosphorylated tau and its reduction to iron (II) reverses the aggregation: implications in the formation of neurofibrillary tangles of Alzheimer's disease. J. Neurochem. *82*, 1137–1147.

Yang, X., Chen-Barrett, Y., Arosio, P., and Chasteen, N.D. (1998). Reaction paths of iron oxidation and hydrolysis in horse spleen and recombinant human ferritins. Biochemistry *37*, 9743–9750.

Zecca, L., Youdim, M.B., Riederer, P., Connor, J.R., and Crichton, R.R. (2004). Iron, brain ageing and neurodegenerative disorders. Nat. Rev. Neurosci. *5*, 863–873.